Cement & Concrete Composites 33 (2011) 46–54

Contents lists available at ScienceDirect

Cement & Concrete Composites

journal homepage: www.elsevier.com/locate/cemconcomp

Evolution of binder structure in sodium silicate-activated slag-metakaolin blends

Susan A. Bernal [a,*], John L. Provis [b,**], Volker Rose [c], Ruby Mejía de Gutierrez [a]

[a] Materials Engineering Department, Composite Materials Group, CENM, Universidad del Valle, Cali, Colombia
[b] Department of Chemical and Biomolecular Engineering, University of Melbourne, Victoria 3010, Australia
[c] Advanced Photon Source, Argonne National Laboratory, Argonne, IL 60439, USA

ARTICLE INFO

Article history:
Received 16 February 2010
Received in revised form 12 August 2010
Accepted 7 September 2010
Available online 15 September 2010

Keywords:
Alkali-activated slag
Metakaolin
Silicate modulus
Structural evolution
High-resolution X-ray diffraction

ABSTRACT

Structural evolution in pastes produced from alkali silicate-activated granulated blast furnace slag (GBFS)/metakaolin (MK) blends is assessed. In the initial period of the reaction, the addition of MK leads to an increase in the total setting time, reduces the heat release, and affects the reaction mechanism by introduction of a large quantity of additional Al. This effect is more significant when an activating solution with a higher silicate modulus is used, and leads to a slight reduction in the final mechanical strength of mortars but a significant increase in setting time, which is valuable in the development of alkali-activated slag binders as these are known to sometimes harden more rapidly than is desirable. High-energy synchrotron X-ray diffractometry reveals that the main reaction products in alkali-activated GBFS/MK blends are segregated and partially crystalline calcium silicate hydrate and aluminosilicate phases, including a small component with a zeolitic (gismondine) structure. No hydrotalcite-type phases are observed in these samples, which are synthesized from a low-Mg slag. A secondary reaction product (Na-substituted C–S–H) is also identified in pastes activated with a modulus of solution of 2.0. Infrared spectroscopy carried out over a period of 180 days shows the development of the gel structure, with aluminum incorporation leading to an increase in the extent of crosslinking, and higher alkalinity giving a more depolymerized gel structure.

1. Introduction

Alkali-activated binders are a class of materials that use an alkaline activator in conjunction with a solid (usually pozzolanic or cementitious) silicate powder to initiate a reaction sequence which results in the formation of a solid material with properties comparable to traditional hydraulic cements [1]. The possible value of alkali-activated binders has been reported since the 1940s [2,3], although it was not until the 1960s that the understanding of the chemistry of these materials began to be established [3–5]. More recent advances in instrumentation, particularly in the areas of electron microscopy, nuclear magnetic resonance spectroscopy and synchrotron radiation-based analysis [6–11], have provided the ability to understand alkali-activated binders on a detailed level, which is essential to the understanding and prediction of their performance and durability.

Of the different materials that have been subjected to alkali activation, granulated blast furnace slag (GBFS) has been the most widely studied, and alkali-activated binders based on GBFS have been used in large-scale applications in regions including Eastern Europe and China [1]. The dominant binder phases in these systems are generally identified to be calcium silicate hydrate (C–S–H) gels which are relatively low in Ca. It is also becoming increasingly apparent that a combination of the properties of "geopolymer"-like (alkali aluminosilicate) and GBFS-based systems can show advantages over either of the end-member systems in terms of the formation of desirable microstructures and mechanical properties [12–18], and so this work is focused on one such system: a blend of GBFS with a small amount of MK, activated by sodium silicate (waterglass) solution. The primary reason for blending MK with GBFS in this study is to provide better control of setting time; slag–waterglass binders have a tendency to set extremely rapidly, and it has been observed that the addition of a small amount of MK can retard setting to provide a more convenient period of workability [19].

There exist only a few previous reports regarding the structure and performance of alkali-activated GBFS/MK blends, and these are mainly focused on the MK-rich end of the continuum, where some GBFS is added to a metakaolin-based geopolymer to enhance strength development [14–16,19,20]. Yip et al. and Buchwald et al. [15,16,20] have observed that at low or moderate activator concentrations in alkali silicate-activated GBFS/MK blends rich in MK, the calcium dissolves from the slag and participates in the formation of C–S–H gels (as has also been observed in MK/$Ca(OH)_2$

* Corresponding author. Present address: Instrument Centre for Solid-State NMR Spectroscopy and Interdisciplinary Nanoscience Centre, Department of Chemistry, Aarhus University, DK-8000 Aarhus C, Denmark. Tel.: +61 3 8344 8755; fax: +61 3 8344 4153.
** Corresponding author. Tel.: +61 3 8344 8755; fax: +61 3 8344 4153.
E-mail addresses: susana.bernal@gmail.com (S.A. Bernal), jprovis@unimelb.edu.au (J.L. Provis).

0958-9465/$ - see front matter © 2010 Elsevier Ltd. All rights reserved.
doi:10.1016/j.cemconcomp.2010.09.004

blends [21,22]) instead of contributing to the formation of geopolymer-type gels. Portlandite ($Ca(OH)_2$) is rarely observed in alkali-activated slag or slag–Portland cement systems beyond early ages, as the high availability of silica in these systems favors instead the formation of C–S–H.

Raw materials with depolymerized siliceous structures, such as GBFS, exhibit higher dissolution rates under high alkalinity conditions when compared with raw materials composed of laminar structures, such as MK. Thus, blending these components can contribute to improving the stability of the system, and potentially also to the durability, when compared to binders prepared from a sole raw material [14,15,19], similar to the advantages in long-term performance provided to Portland cement-based systems by the addition of slower-reacting pozzolans in addition to rapidly-reacting cement.

However, slag-rich GBFS/MK blends have shown quite rapid carbonation under accelerated test conditions [19,23], and so it is necessary to develop a better understanding of the progress of the binder formation reactions and of the final hydration products in these materials to enable binder design for enhanced durability. Different sodium silicate activator compositions, and different degrees of MK substitution into the slag-rich formulations, are analyzed here through the application of calorimetry, synchrotron X-ray diffraction and Fourier transform infrared spectroscopy, to determine the details of phase formation and structural development during 180 days of curing. Compressive strength testing is conducted on mortar samples based on the binders developed, in order to generate a better understanding of the relationship between the structural evolution of the pastes and the mechanical strength at different ages of curing.

2. Experimental program

2.1. Materials

The primary raw material used in this study was a Colombian granulated blast furnace slag (GBFS) obtained from the *Acerías Paz del Río* steelworks. The basicity coefficient ($CaO + MgO/SiO_2 + Al_2O_3$) and the quality coefficient ($CaO + MgO + Al_2O_3/SiO_2 + TiO_2$) based on the chemical composition (Table 1) were 1.01 and 1.92, respectively. Its specific gravity was 2900 kg/m^3 and its Blaine fineness 399 m^2/kg. The particle size range, determined through laser granulometry, was 0.1–74 μm, with a mean (d_{50}) of 5 μm.

The metakaolin (MK) used was generated in the laboratory by calcination of a Colombian kaolin (containing minor quartz and dickite impurities) at 700 °C in air, for 2 h. The particle size range of the MK was 1.8–100 μm, with a d_{50} of 13.2 μm and 10% of particles finer than 4 μm.

Mineralogical analysis of the anhydrous raw materials was conducted by synchrotron X-ray diffractometry (Fig. 1).

It can be seen from Fig. 1 that the slag is mainly amorphous, as seen by the broad feature in the diffraction pattern at *Q* values between 1 and 3 Å^{-1}. Traces of some crystalline phases such as gehlenite ($Ca_2Al_2SiO_7$) (Powder diffraction file (PDF) # 035-0755), quartz (SiO_2) (PDF# 046-1045) and calcite ($CaCO_3$), (PDF# 05-0586) are also observed. In this case akermanite ($Ca_2MgSi_2O_7$), a mineral often reported in slags used for alkali-activation purposes, is not identified. This is probably a consequence of the low (<3%) content of magnesium in the slag assessed here.

Table 1
Oxide composition of the GBFS and MK used, from X-ray fluorescence analysis. LOI is loss on ignition at 1000 °C.

Component (mass% as oxide)	GBFS	MK
SiO_2	32.29	50.72
Al_2O_3	16.25	44.63
CaO	42.45	2.69
Fe_2O_3	2.35	–
MgO	2.87	–
Other	1.88	0.94
LOI	1.91	1.02

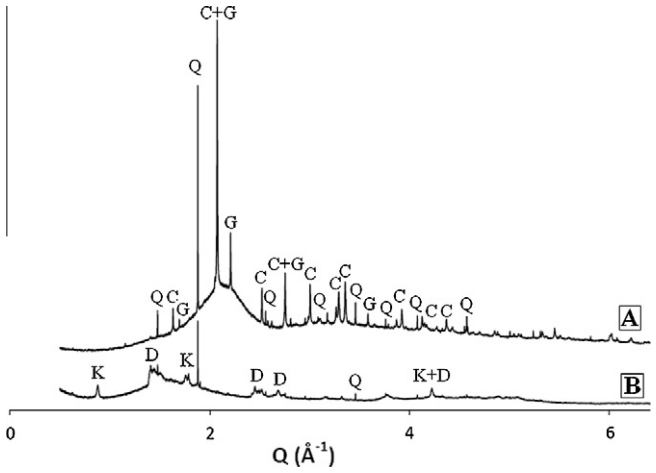

Fig. 1. High resolution synchrotron X-ray diffraction patterns of: (A) GBFS, and (B) MK (λ = 0.401738 Å), where peaks marked with K are due to kaolinite, D is dickite, Q is quartz. C is calcite and G is gehlenite.

In the diffraction pattern of the MK, the main crystalline phases accompanying the amorphous component of the MK are traces of kaolinite ($Al_2O_3{\cdot}2SiO_2{\cdot}2H_2O$) (PDF# 014-0164), dickite (also $Al_2O_3{\cdot}2SiO_2{\cdot}2H_2O$) (PDF# 010-0446) and quartz (SiO_2) (PDF# 046-1045), being characteristic of clays of moderate purity. It is important to note that the characteristic peaks associated with kaolinite are weak, indicating a high degree of disorder as a consequence of the conversion from kaolin to MK under the heating conditions used to prepare the material in this study [24–27]. Muscovite, feldspars and anatase, which are typically observed in MK with low purity, are not detected in this material.

Alkaline activating solutions were formulated by blending a commercial sodium silicate solution with 32.4 wt.% SiO_2, 13.5 wt.% Na_2O and 54.1 wt.% H_2O, together with 50 wt.% NaOH solution, to reach the desired modulus (Ms = molar SiO_2/Na_2O ratio) of 1.6, 2.0 or 2.4. A constant activator concentration of 5% Na_2O by mass of GBFS + MK was used.

2.2. Sample synthesis and test procedure

2.2.1. Pastes

Pastes with a constant water/(GBFS + MK + anhydrous activator) ratio of 0.23 were produced in accordance with the standard procedure ASTM C305-06. In fresh pastes, setting time was determined using the Vicat apparatus by following the standard procedure ASTM C191-08. The setting process of these mixes was also assessed by isothermal calorimetry (JAF calorimeter) at 25 °C over the first 40 h of reaction.

For the study of hardened pastes, the specimens were cast in cylindrical molds and stored in sealed containers with a relative humidity of 90% and a temperature of 27 ± 2 °C for up to 180 days. The reaction process was stopped at different ages of curing by crushing the samples to pass a 74 μm sieve, submerging the samples in acetone for 15 min, filtering and drying. To prevent the absorption of water or CO_2 from the atmosphere, samples were stored in a desiccator until testing.

X-ray diffractometry was carried out using a high-resolution high-throughput synchrotron powder X-ray diffractometer with a

system of twelve simultaneous analyzer/detectors at beamline 11-BM at the Advanced Photon Source (APS), Argonne National Laboratory, USA. The tests were conducted in accordance with the standard protocols for automated data acquisition on the 11-BM beamline. The conditions for the data collection were: continuous scanning of a detector covering an angular range of 34° with a step rate of 0.01°/s, a step size of 0.001° and a wavelength of $\lambda = 0.401738$ Å. Data have been converted to Q units ($Q = \frac{4\pi \sin\theta}{\lambda}$) for presentation here, to enable more ready comparison with data sets collected at different wavelengths.

Fourier transform infrared (FTIR) spectrometry was conducted via the KBr pellet technique, using a Shimadzu FTIR 8400 instrument, scanning from 2000 to 600 cm^{-1}.

2.2.2. Mortars

Mortars were also produced following the standard procedure ASTM C305-06. River sand with a fineness modulus of 2.75 was used as fine aggregate. All samples were formulated with a constant water/(GBFS + MK + anhydrous activator) ratio of 0.47 and a binder/sand ratio of 1:2.75. While this is quite a high water content for alkali-activated mortars, it was designed to replicate a binder formulation which has been used successfully in the preparation of alkali-activated slag concretes [19]. The specimens were cast in 50.8 mm cubic molds, and stored under controlled relative humidity (RH) ~85% and ambient temperature (~25 °C) for 24 h. Samples were then demolded and cured under RH of 90% and a temperature of 27 ± 2 °C for up to 180 days. Compressive strength testing was conducted at various ages according to ASTM C109.

3. Results and discussion

3.1. Isothermal calorimetry and setting time

Fig. 2 shows the heat evolution from alkali-activated GBFS and GBFS/MK blends, which appears to be in accordance with previous findings for alkali-activated slag systems activated by $Na_2O{\cdot}rSiO_2$ [28–31]. The initial peak (inset in each panel in Fig. 2) observed during the first few minutes of reaction is assigned to the initial pre-induction stage of the hydration process. It should also be noted that mixing was carried out outside the instrument and the mixed pastes then introduced into the instrument for measurement; time zero on the plots represents the time at which the sample was placed in the instrument, which was 3 min after the start of mixing in each case. This initial heat release corresponds to particle wetting, the start of dissolution of the slag particles, the formation of the initial dissolved silicate units and their complexation with calcium and sodium. This occurs at the same point in time in every sample studied, regardless of solids or activator composition, indicating that it is probably attributable to physical rather than specific chemical processes.

There is then in the lower-alkalinity (i.e. higher silica; Ms 2.4) samples a period of limited heat release, generally identified as the induction period. Setting of these samples happens during this period as gelation occurs; the shaded boxes in Fig. 2 highlight the period between the initial and final set as measured by the Vicat method.

The second main peak (acceleration and deceleration) identified at advanced times of reaction seems to be highly dependent on the alkalinity of the activator, and is related to the massive precipitation of reaction products, mainly C–S–H gel (with substitution of other elements) and other products with more complex composition, which will be identified in detail later in this paper.

The unblended alkali-activated slag sample (Fig. 2A) with Ms 2.4 shows a very distinct induction period. The presence of an induction period in alkali-activated binders can be a consequence of the combination of two phenomena: the inhibition of the reaction as result of the precipitation of reaction products over the surfaces of unreacted grains of slag [29–31] and the time required to reach a critical concentration of ionic species in the system in order to form reaction products [32–34]. The end of the induction period appears after 114 min, and the start of the acceleration stage is

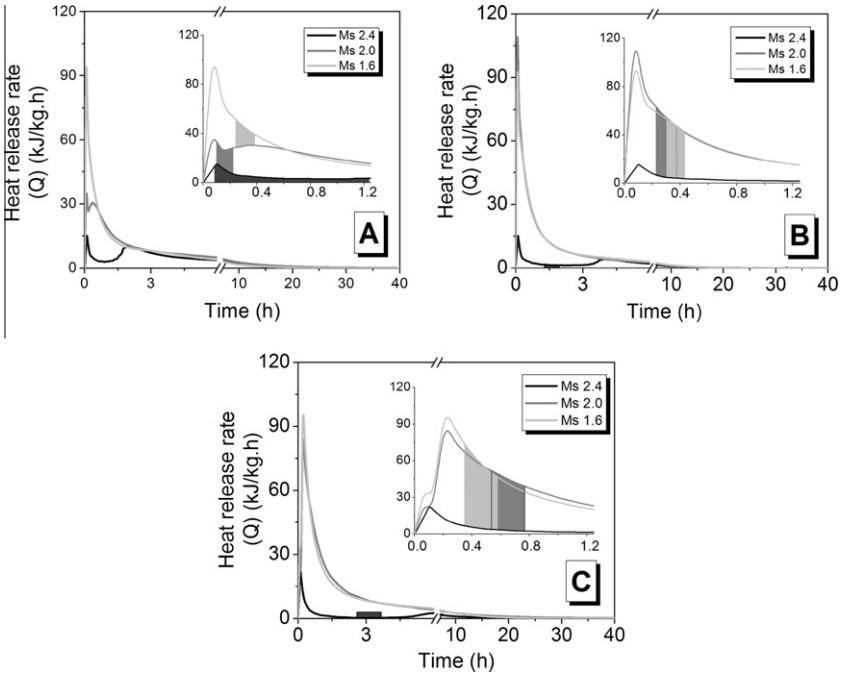

Fig. 2. Heat release from alkali-activated GBFS/MK blends with GBFS/(GBFS + MK) ratios of: (A) 1.0, (B) 0.9 and (C) 0.8. The highlighted areas in the inset panels, and on the main plot in each case for the Ms 2.4 samples, corresponding to the setting period (from initial set to final set) determined for each mix by the Vicat test. Shading colors correspond to line colors for the each data set.

coincident with the final setting time of these samples, which is consistent with the behavior of conventional cements [35,36].

A decrease in Ms to 2.0 (medium-gray data set in Fig. 2A) leads to a shift to lower times of the acceleration–deceleration peak, so that no induction period is identified; however, the two peaks are still distinct. For this sample, similar to the Ms 2.4 sample, the initial set coincides with the maximum in the initial heat release peak. However, the final setting time of the Ms 2.0 sample corresponds to the maximum in the second peak, where the deceleration period is starting. These results suggest that an increase in the alkalinity of the system could be leading to a more rapid dissolution of the slag and consequently to a greater degree of precipitation of reaction products earlier in the reaction process. The same trend was observed in pastes prepared with Ms 1.6, which display a single peak assigned to the acceleration process. Under these activation conditions the reaction takes place so quickly that the pre-induction and induction periods cannot be detected.

During alkali activation, the alkalinity of the activator leads to the release of Ca, Si and Al from the slag. The ions that are released from the slag glass particles must then diffuse through the exterior layer of hydrate reaction products which rapidly forms around the unreacted slag particles [37]. The alkaline conditions accelerate the reaction process of activation [38], as the presence of OH^- enhances slag dissolution, and also increases the solubility of silica and alumina. This suggests that activators with lower Ms (and therefore higher OH^- concentration) contribute more strongly to the dissolution of the slag, leading to reduction of setting times. These results are coherent with those observed by Bakharev et al. [39]. The setting times observed here are in general lower than those reported by Fernández-Jiménez and Puertas [38] for similar activation conditions, which is most likely attributable to differences in the chemical compositions and particle size distributions of the slag sources. The slag studied here has a lower Mg content and a lower Si/Al ratio than the slag studied by those authors, which may be significant.

The heat released by pastes with a GBFS/(GBFS + MK) ratio of 0.9 (Fig. 2B) also decreases with increasing Ms, similar to the trend reported for samples based solely on slag; however, the total heat released when MK is incorporated in the binder is substantially reduced. Additionally, an important increase in the setting time, particularly when activation is carried out with Ms 2.4, is identified. In this high-silica sample, the initial and final setting times both fall during the induction period, suggesting that the setting time measured by the Vicat test is not an accurate indication of the formation of the majority of the binder phases, because the main precipitation of bulk reaction products takes place after setting has already occurred. In samples activated with Ms 2.0 and 1.6, on the other hand, the setting time is reported during the acceleration/deceleration period. The Vicat test is, as a simplification of its physics, measuring the point in time at which the yield stress passes a certain value (approx. 40 kPa for initial setting of pastes, according to the analysis of Lootens et al. [40]). These results suggest that there are important differences in yield stress development between mixes of different alkalinity, which impact the ability to correlate the extent of microstructure formation (as measured by rheology) with the extent of gel nanostructure formation (as measured by calorimetry).

Samples prepared with an increased MK content in the binder (GBFS/(GBFS + MK) = 0.8; Fig. 2C), with Ms 1.6 or 2.0, exhibited an initial shoulder in the acceleration/deceleration period, which can be related to the pre-induction heat release peak appearing after 4 min. Under these activation conditions, the initial and final setting times fall during the deceleration period. However, increasing Ms to 2.4 leads to a completely different behavior compared with the other activation conditions assessed. The calorimetry data reveal an initial peak related to the pre-induction processes at around 4 min, similar to the more alkaline samples, but this is then followed by a long induction stage of ~3 h. A second, small heat release peak is identified after 6 h. In this case the initial and final setting times coincide approximately with the end of the induction period and the early part of the acceleration stage. These results are coherent with the trends observed in samples with 10% MK (Fig. 2B), and suggest that an increased MK content in the binder leads to the inhibition of the reaction kinetics, which could negatively affect early age mechanical strength.

Alkalinity is reasonably high throughout the reaction process in all systems studied, which in blended binders will supply the necessary conditions to initiate MK dissolution. However, dissolution–condensation processes involving GBFS and MK take place simultaneously, and the formation of reaction products reduces the available amount of alkalis in the system because they participate in the chemical reaction and formation of aluminosilicate gels [41], inhibiting the subsequent dissolution of MK. Based on this, it is suggested that the kinetics of reaction of GBFS/MK blends under these activation conditions may be slowed over the first few hours as a consequence of alkalinity variations, in addition to the mass transport limitations introduced by the formation of reaction products.

It is also important to note that under the activation conditions assessed here, the setting times of all mixes fall between 5 min and 48 min (Table 2), is substantially lower than those conventionally reported for ordinary Portland cement [35,36]. This behavior should be taken into account in the industrial application of these materials.

3.2. Compressive strength

Fig. 3 shows that an increased MK content in the binders leads to a reduction of compressive strength, this effect being more significant when a higher Ms activator is used. A decrease in the final strength with MK addition was noted in a previous study of the carbonation behavior of these materials [23], and also in another recent study spanning the full range from pure-GBFS to pure-MK systems [42], although the trend does not necessarily extend to very MK-rich materials [14]. However, it is interesting to note that the percentage of the final strength achieved at each curing duration does not change significantly with the addition of MK, i.e., the relative strength development profile remains similar even while the final strength changes.

The Ms 2.0 samples were consistently stronger than the Ms 2.4 samples at all ages and at each level of MK substitution. However, reliable data for the Ms 1.6 activator were not able to be generated due to the very poor workability of these mixes.

All the mortars assessed show mechanical strengths of at least 40 MPa after 7 days of curing, reaching final strengths up to 74 MPa for samples based solely on alkali-activated slag, which falls in the range characteristic of the type of binder which can

Table 2
Setting times of all mixes analyzed, as measured by the Vicat method.

Ms	GBFS/(GBFS + MK) ratio	Initial setting time (S_{ti}) (h)	Final setting time (S_{tf}) (h)	Total setting time (h) = $S_{tf} - S_{ti}$
2.4	1.0	0.93	1.22	0.28
2.0		0.23	0.38	0.13
1.6		0.13	0.22	0.08
2.4	0.9	1.48	1.83	0.35
2.0		0.23	0.37	0.13
1.6		0.30	0.45	0.15
2.4	0.8	2.82	3.62	0.80
2.0		0.55	0.78	0.22
1.6		0.38	0.58	0.22

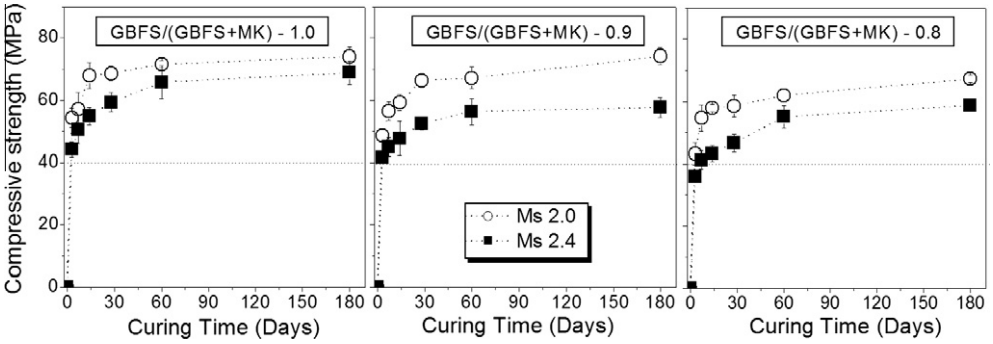

Fig. 3. Compressive strength of mortars based on silicate-activated GBFS/MK blends. Data are reported as average and standard deviation of three replicate tests; error bars where not shown are smaller than the data symbols.

be used to produce high performance concrete. This behavior is attributable to the chemical reactions that take place during alkaline activation, which are controlled by diffusion and precipitation mechanisms with faster kinetics than the diffusion controlled reactions in the hydration of ordinary Portland cement [43,44], in accordance with observations from calorimetry. Also, none of the samples showed the strength regression which is sometimes observed in poorly-formulated or poorly-cured alkali-activated binders.

3.3. Synchrotron XRD analysis

Fig. 4 shows that for GBFS activated with Ms 2.4, the major X-ray crystalline phases are gehlenite ($Ca_2Al_2SiO_7$), quartz (SiO_2) and calcite ($CaCO_3$) contributed by the unreacted slag. The slag was slightly weathered before use, which is the reason for the presence of calcite. Two crystalline reaction products are also identified: a calcium silicate hydrate (C–S–H) ($Ca_6Si_3O_{12}{\cdot}xH_2O$) (PDF# 014-0035) and the aluminosilicate zeolite gismondine ($CaAl_2Si_2O_8{\cdot}4H_2O$) (PDF# 020-0452). The observed phases are in accordance with those reported by other studies [4,6,44–49] when slag is activated with sodium silicate solutions, except that gismondine is only rarely observed [23,50]. This phase is only able to be identified in the current study due to the extremely high resolution of the synchrotron X-ray diffractometer used; the peaks assigned to this phase are small but sharp, and would be difficult to distinguish by laboratory X-ray diffraction. All diffractograms also show a relatively strong contribution from non-crystalline components, but it is not possible to distinguish the amorphous C–S–H gel phases from the unreacted slag in these data sets.

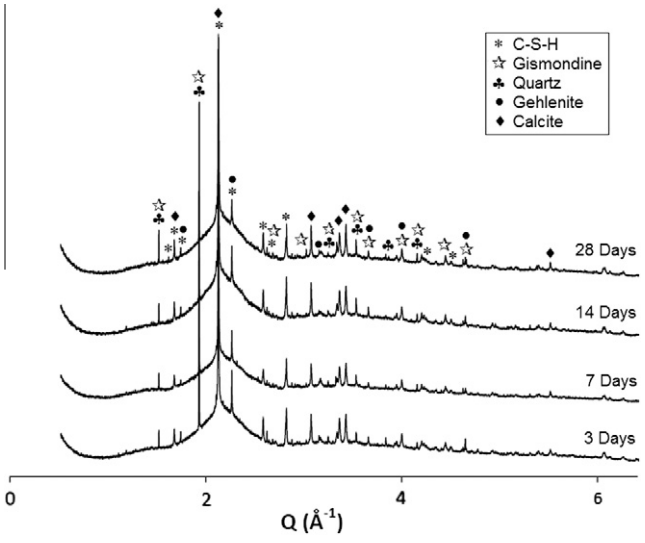

Fig. 4. High resolution synchrotron X-ray diffraction patterns of pastes (λ = 0.401738 Å) based on alkali-activated GBFS with Ms = 2.4, at different ages of curing.

No crystalline hydrotalcite-type phases are observed in any of the samples studied in this investigation, which is attributable to the very low Mg content of the slag used. The effect of the Mg content of the slag on the formation of hydrotalcite-type phases has received relatively little attention in the literature, as the majority of European and North American slags which have been subjected to alkali activation have had a fairly consistent 7–10% MgO content, compared to <3% here. Within the quaternary oxide system $CaO–MgO–SiO_2–Al_2O_3$, when it is necessary to omit one component to enable the system to be plotted on a ternary phase diagram for discussion of slag chemistry in alkali activation (or in blending with Portland cements), the omitted component is almost always MgO. However, the results obtained here show that this component can actually have a significant influence on the chemical and molecular structure of the binder phase – and the importance of this observation extends not only to the presence or absence of a discrete hydrotalcite phase, as this phase (when present) is intimately intermixed on a nanometer length scale with the C–S–H gel which dominates the binder and controls its mechanical performance [6].

As curing time is increased, samples activated with Ms 2.4 (Fig. 4) shows an increase in the intensity of the peaks around Q = 1.47, 1.88, 2.56, 3.19, 3.49 and 4.08 Å^{-1}, which are overlapping peaks in the quartz and gismondine patterns. During the early stages of curing (up to 7 days), the changes in the intensity of the peaks are probably a consequence of partial reaction of the quartz that was present in the unreacted slag. However, the absence at advanced curing durations of a peak at Q = 3.78 Å^{-1}, the reduction in the intensity of the peak around Q = 11.7 Å^{-1} (which is identified in the pattern of samples with 3 days of curing and is associated with quartz), and the formation of new peaks at Q = 2.75, 3.30 and 4.38 Å^{-1} corresponding to gismondine at 28 days of curing, show that advanced ages of curing contribute to the formation of zeolitic phases. A similar trend regarding the overlapping gehlenite/gismondine peaks at Q = 4.60 and 3.57 Å^{-1} is also notable. In this case a decrease in the peak around Q = 3.08 Å^{-1} at advanced ages of curing suggests that the formation of the alkali-activated binder phase is also consuming some of the crystalline gehlenite supplied by the slag. It is additionally noted that one of the main peaks of gismondine (Q = 2.97 Å^{-1}) is not observed at early ages of curing, which suggests that the development of full crystallinity in this phase requires advanced ages of curing as a consequence of its complex structure. Such differences in the rate

of appearance of different peaks assigned to zeolite structures are reasonably commonly observed when the zeolites are being formed as a component of an alkali-activated binder.

Increased intensity of the peaks attributed to crystalline C–S–H is observed at higher ages of curing. The positions of the peaks associated with this phase are slightly shifted when compared with those identified for a tobermorite-type calcium silicate hydrate (riversideite-9 Å, ($Ca_5Si_6O_{16}(OH)_2$) (PDF#029-0329)), which suggests that there is some coherence between the structure of the C–S–H obtained in these mixes and riversideite-9 Å, but that some elements of the structures do differ (possibly the Ca/Si ratio and/or bound water content). The peaks due to calcite do not show any variation with the time of curing, indicating that this compound is formed from the weathering of unreacted slag and is not involved to a significant extent in the alkali-activation process, as has been observed previously for low levels of calcite added to an alkali-silicate activated MK binder [51].

In GBFS/MK blends (Fig. 5), the same phases and trends observed in Fig. 4 for pastes based solely on GBFS activated under the same conditions (Ms) are identified. In this case it seems that the addition of MK in the binder modifies the growth process predominantly on a microstructural level, because clear differences in phase formation is not observed when comparing the two data sets. This could be a consequence of the low dissolution of MK under these relatively low-alkalinity conditions, or it may be that all the products which are specific to reactions involving MK are very poorly crystalline. It is noted that coherent with the increase in compressive strength during curing (Fig. 3), the intensities of the C–S–H peaks (Q = 1.47, 1.61 and 1.69 Å^{-1}) and gismondine peaks (Q = 1.88 and 2.56 Å^{-1}) increase slightly with time as well.

Pastes activated with Ms 2.0 (Fig. 6) show, in addition to the major X-ray crystalline phases contributed by the unreacted slag, and the C–S–H and gismondine as identified in the higher-silica samples, a secondary C–S–H product enriched in Na^+ (sodium-calcium silicate hydrate, $Na_2Ca_2Si_2O_7{\cdot}H_2O$, termed Na–C–S–H; PDF#00-022-0891). Higher ages of curing give an increase in the intensity of the peaks at Q = 1.64, 2.18 and 3.57 Å^{-1} related to the distinct Na–C–S–H phase, along with the formation of peaks around Q = 2.86 and 4.19 Å^{-1} which are solely assigned to this phase. An increase in the intensity of some peaks related to crystalline C–S–H (Q = 1.93 Å^{-1} and 2.18) is identified, as well as a new series of low intensity peaks in the region of Q = 2.43 to 2.45 Å^{-1},

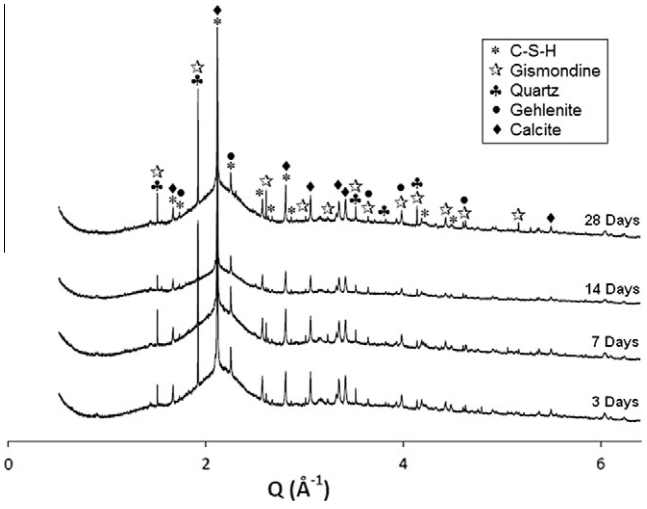

Fig. 5. High resolution synchrotron X-ray diffraction patterns of pastes (λ = 0.401738 Å) based on alkali-activated GBFS/10% MK blends with Ms = 2.4, at different ages of curing.

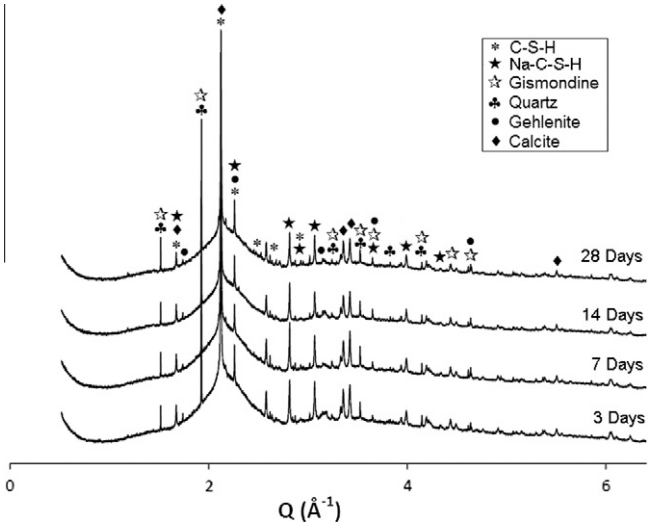

Fig. 6. High resolution synchrotron X-ray diffraction patterns of pastes (λ = 0.401738 Å) based on alkali-activated GBFS with Ms = 2.0, at different ages of curing.

associated with the Na–C–S–H phase. These results suggest that at advanced ages of curing, the hydration products formed might present a slightly higher degree of crystallinity, but also show that extensive formation of additional crystal phases with longer curing durations, as is sometimes observed in alkali-activation systems based on fly ash or metakaolin, is not observed. The main peaks of calcite at Q = 2.97, 3.24 and 3.30 Å^{-1} exhibited a reduction in intensity in this sample, and the absence of the gehlenite peaks around Q = 3.06 and 3.13 Å^{-1} is also observed.

These results indicate that the increased alkalinity associated with lower Ms is leading to the formation of C–S–H gels which are more complex and enriched in Na^+. It may also be that the lower Si content of the activating solution is playing a role in this, with the formation of less Si-rich gels providing more opportunities for incorporation of Na^+ onto the sites which would usually be filled by Ca^{2+} in C–S–H gels derived from (very Ca-rich) Portland cements. Previous studies regarding the effects of these phases on the carbonation behavior of the pastes assessed in this study [23] suggest that the formation of Na–C–S–H might reduce the susceptibility to carbonation of these binders, as component migration to balance the charges in decalcified C–S–H gel (the main compound affected by carbonation in alkali-activated slag systems) could be occurring, instead of the formation of sodium carbonates.

In mixes with a GBFS/(GBFS + MK) ratio of 0.9 and Ms 2.0 (Fig. 7), the same crystalline phases previously observed in Figs. 5 and 6 are again present. However, in this case, a significant increase in the intensities of some of the main peaks related to the Na-C-S-H (Q = 1.64, 2.18, 2.56 and 3.54 Å^{-1}) and gismondine (Q = 3.40 and 4.06 Å^{-1}) can be identified at advanced ages of curing. This suggests that under conditions of sufficient alkalinity to generate significant dissolution of MK during binder formation, the increase in the amount of dissolved Al^{3+} and Na^+ in the system will contribute to the formation of Al or Na-enriched phases.

3.4. FTIR

Fig. 8 shows infrared spectra for slag-only samples at various ages of curing. All infrared band assignments presented in this discussion follow references [52–57].

Curing for longer durations predominantly affects the band at around 1000 cm^{-1}, assigned to the asymmetric stretching mode of the Si–O–T (T = tetrahedral Si or Al) bonds within the reaction

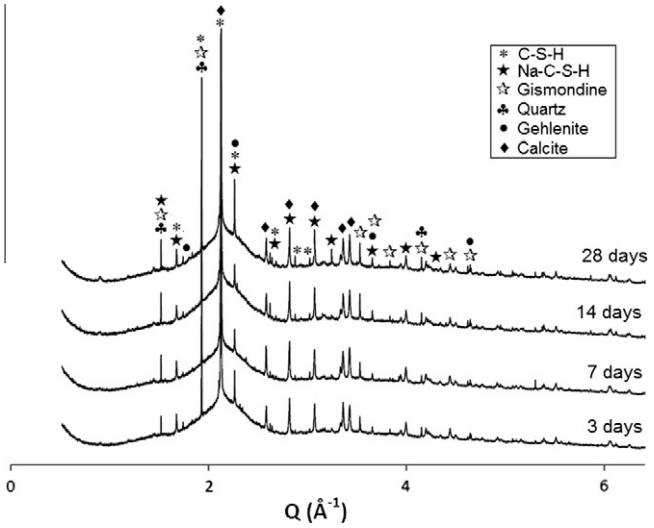

Fig. 7. High resolution synchrotron X-ray diffraction patterns of pastes (λ = 0.401738 Å) based on alkali-activated GBFS/10% MK blends with Ms = 2.0, at different ages of curing.

products [52,53] and identified in the anhydrous slag. Samples cured for 7 days exhibit a strong but broad band at 980 cm^{-1}, associated with a highly depolymerized silica network and attributed mainly to the contribution of the unreacted slag at the earlier stages of reaction. After 28, 90 and 180 days a shift in this band to 990 cm^{-1}, 994 cm^{-1} and then 1002 cm^{-1} was observed, with an apparent sharpening between 28 and 90 days as the contribution from the unreacted slag peak diminishes. An increased wavenumber of the asymmetric stretching band of Si–O–T bonds in C–S–H gels correlates with increased polymerization degree [57]. The higher intensities of these bands after 90 and 180 days of curing also show a greater extent of reaction product formation at these ages of curing, which contributes positively to the development of a higher mechanical strength at advanced ages of curing (Fig. 3). The broad and weak band at 710–715 cm^{-1} corresponds to the bending of Al–O–Si bonds in ring structures [55,56]. The shoulder at 876 cm^{-1} is associated with the asymmetric stretch of AlO_4^- groups, and the mode at 715 cm^{-1} corresponds to the bending of Al–O–Si bonds [52,53].

Pastes based solely on GBFS activated with Ms 2.4 (Fig. 8A) show vibrational bands at 1663 cm^{-1} and 1642 cm^{-1}, assigned to the bending of H–OH bonds of free water (1663 cm^{-1}) and chemically bound water (1642 cm^{-1}) [57]. A decrease in this band with increasing age of curing is identified, so that in samples after 90 and 180 days this vibration mode is almost imperceptible. Increased intensity with time was observed in the bands between 1443 cm^{-1} and 1440 cm^{-1} related to the asymmetric stretching mode of the O–C–O bonds of CO_3^{2-} groups [54]. This suggests that some superficial carbonation of the samples could have taken place during curing, but probably by physical mechanisms rather than chemical reaction as no growth in crystalline carbonate phases was observed by XRD (Fig. 4). Although care was taken to prevent this, it has previously been shown that these materials are quite highly prone to carbonation [23].

The spectra of samples activated with Ms 2.0 are presented in Fig. 8B. Under these more alkaline activation conditions, the asymmetric stretching mode of Si–O–T bonds is observed at lower wavenumber (~980 cm^{-1}) when compared with the samples activated with Ms 2.4. This suggests that a reduced Ms leads to a reaction product with higher Ca/Si ratio and thus a lower degree of polymerization than those obtained when activation is carried out at higher Ms. The initial peak due to the slag is at low wavenumber as in Fig. 8A, but in this case moves to a lower wavenumber (971 cm^{-1}) at 28 days, as the availability of calcium from the slag precursor is very high, before moving to 981 cm^{-1} by 90 days as the degree of polymerization of the binder increases and more silicon from the slag particles is incorporated. However, this peak then changes only slightly in position from 90 to 180 days, indicating that the degree of polymerization (and potential substitution of Si by Al) in the reaction products is not changing significantly at advanced ages, which is consistent with the absence of further mechanical strength development during this time period (Fig. 3). Systematic differences in the carbonate peak around 1440 cm^{-1} are not observed at the different ages of curing in this mix, although the 28 day sample shows an apparent shift in the peak to 1430 cm^{-1} which cannot be straightforwardly explained except as instrumental noise in this spectral region.

GBFS/MK blends activated with Ms 2.4 (Fig. 9A) show similar spectra to those obtained for samples based solely on GBFS under the same activation conditions (Fig. 8A). The shift in the asymmetric stretching mode of the Si–O–T bonds (from 976 cm^{-1} at 7 days to ~1000 cm^{-1} subsequently) is more rapid than in the samples without MK, but the peak position after 7 days is at a lower wavenumber (976 cf. 980 cm^{-1}) in the sample with MK. This lower wavenumber at 7 days is symptomatic of a lower degree of reaction, and agrees with the observation that the incorporation of

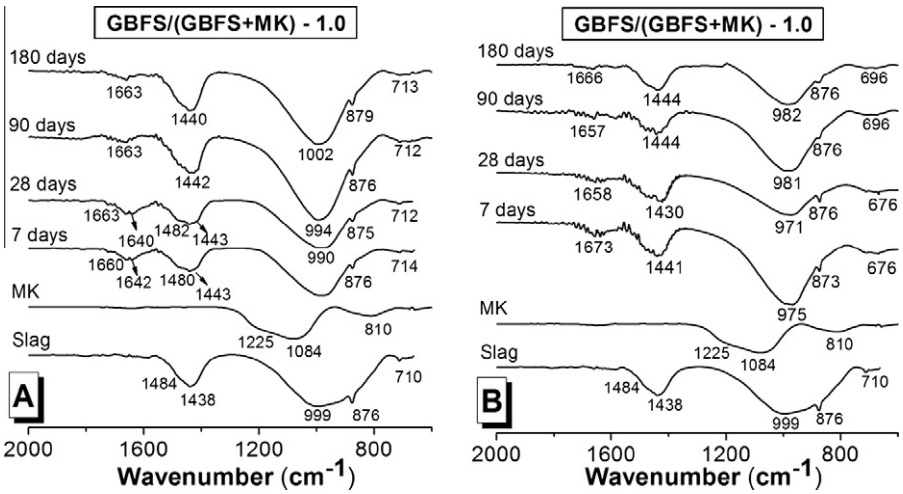

Fig. 8. Fourier transform infrared spectra of pastes of GBFS activated with (A) Ms = 2.4 and (B) Ms = 2.0 as a function of the curing age.

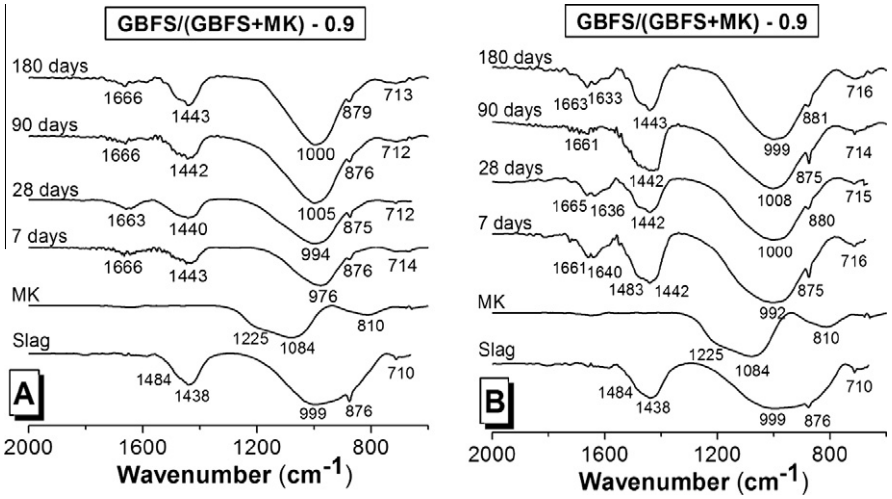

Fig. 9. Fourier transform infrared spectra of pastes of GBFS/MK blends (10% MK) activated with (A) Ms = 2.4 and (B) Ms = 2.0 as a function of the curing age.

MK retards the polymerization of the reaction product in the very early period of reaction, as identified in this system through calorimetry (Fig. 2). The more rapid shift to a higher wavenumber at 28 days is then related to the influence of the Al supplied by the MK in enhancing the degree of polymerization. At advanced ages of curing, the band assigned to the Si–O–T bonds is observed at a wavenumber comparable to those previously reported for pastes prepared solely with GBFS; the effects of Al in enhancing polymerization (giving an increase in the wavenumber) and modifying the chemistry of the Si–O–T bonds (giving a decrease in the wavenumber) appear to counteract each other to some extent.

In binders with a GBFS/(GBFS + MK) ratio of 0.9 activated with Ms 2.0 (Fig. 9B), the intensity of the ~1442 cm^{-1} carbonate vibration has increased markedly when compared with the samples based solely on GBFS at the same ages of curing (Fig. 8). This is consistent with the previously observed differences in carbonation behavior [23]; this sample has been observed to carbonate very rapidly in accelerated testing.

The asymmetric vibration mode related to Si–O–T bonds (992–1008 cm^{-1}) is broader was observed in samples activated with Ms 2.4, with a more distinct shoulder on the high wavenumber side, and also begins to shift to lower wavenumbers with increased age of curing. This indicates the formation of reaction products with a high degree of polymerization (the 1008 cm^{-1} peak at 90 days is the highest observed for any sample in this study), and that incorporation of more Al into the reaction products at extended curing durations then leads to a reduction in wavenumber at 180 days, coherent with the higher eventual dissolution of MK expected under these more alkaline activation conditions. The high-wavenumber shoulder indicates the presence of some form of segregated Si-rich gel phase. While it is not immediately clear why this should be present in this, the lowest-silica sample of all those studied, it is possible that this could be due to the silica layers from dealuminated remnant metakaolin particles, similar to what has previously been suggested in the synthesis of aluminosilicate 'geopolymers' from metakaolin [58].

4. Conclusions

Analysis of alkali silicate-activated slag/metakaolin blends shows strong dependence of material properties on the silica modulus (molar SiO_2/Na_2O ratio) of the activating solution. Higher-modulus (2.4) samples present lower mechanical strength, slower setting and less heat release compared with samples formulated with a lower solution modulus. The main reaction products are a partially crystalline C–S–H gel and a gismondine-group zeolite in all samples, with an additional Na-substituted C–S–H phase observed by X-ray diffractometry in samples activated with a silica modulus of 2.0. Hydrotalcite-type phases are not observed in any sample analyzed here, which is attributed to the very low Mg content of the slag source used.

The effect of small amounts (10–20%) of metakaolin on the alkali-activation process appears to be mostly related to the provision of additional aluminum to the reacting system. Infrared spectroscopy shows significant differences in silicate gel chemistry when metakaolin is added, with a higher degree of incorporation of Al into the C–S–H gel structure and a more polymerized gel structure formed. Addition of metakaolin decreases the final strength slightly, but does not change the relative strength development profile (the fraction of final strength developed at each point in time). Metakaolin also provides added workability and extends the setting time, which is of significant value in the application of alkali-activated slag binders due to their sometimes inconveniently short pot life.

The information developed in this study will be very beneficial in understanding and enhancing the durability – and particularly the carbonation resistance – of alkali-activated slag binders both with and without metakaolin addition. The alkali-rich nature of the C–S–H gels which dominate the binder in these systems has previously been observed to cause differences in degradation mechanisms and products when compared to traditional cement-based binder systems, and knowledge of the processes which control the phase composition of these new binders is now able to be used to tailor formulations and binder structures for improved performance in desired areas.

Acknowledgements

This study was sponsored by *Universidad del Valle* (Colombia), *Instituto Colombiano para el Desarrollo de la Ciencia y Tecnología "Francisco José de Caldas"* (COLCIENCIAS) and the Centre of Excellence of Novel Materials (CENM). Use of the Advanced Photon Source at Argonne National Laboratory was supported by the US Department of Energy, Office of Science, Office of Basic Energy Sciences, under Contract No. DE-AC02-06CH11357. The participation of JLP was funded by the Australian Research Council (ARC), including partial funding through the Particulate Fluids Processing Centre, a Special Research Centre of the ARC.

References

[1] Shi C, Krivenko PV, Roy DM. Alkali-activated cements and concretes. Abingdon, UK: Taylor and Francis; 2006.
[2] Purdon AO. The action of alkalis on blast-furnace slag. J Soc Chem Ind-Trans Commun 1940;59:191–202.
[3] Roy D. Alkali-activated cements – opportunities and challenges. Cem Concr Res 1999;29(2):249–54.
[4] Puertas F. Cementos de escoria activados alcalinamente: situación actual y perspectivas de futuro. Mater Construcc 1995;45(239):53–64.
[5] Wang S-D, Pu X-C, Scrivener KL, Pratt PL. Alkali-activated slag cement and concrete: a review of properties and problems. Adv Cem Res 1995;7(27): 93–102.
[6] Richardson IG, Brough AR, Groves GW, Dobson CM. The characterization of hardened alkali-activated blast-furnace slag pastes and the nature of the calcium silicate hydrate (C–S–H) paste. Cem Concr Res 1994;24(5):813–29.
[7] Wang S-D, Scrivener KL. ^{29}Si and ^{27}Al NMR study of alkali-activated slag. Cem Concr Res 2003;33(5):769–74.
[8] Provis JL, Lukey GC, van Deventer JSJ. Do geopolymers actually contain nanocrystalline zeolites? – a reexamination of existing results. Chem Mater 2005;17(12):3075–85.
[9] Provis JL, Rose V, Bernal SA, van Deventer JSJ. High resolution nanoprobe X-ray fluorescence characterization of heterogeneous calcium and heavy metal distributions in alkali activated fly ash. Langmuir 2009;25(19): 11897–904.
[10] Lloyd RR, Provis JL, Smeaton KJ, van Deventer JSJ. Spatial distribution of pores in fly ash-based inorganic polymer gels visualised by Wood's metal intrusion. Micropor Mesopor Mater 2009;126(1–2):32–9.
[11] Richardson IG. Tobermorite/jennite- and tobermorite/calcium hydroxide-based models for the structure of C–S–H: applicability to hardened pastes of tricalcium silicate, β-dicalcium silicate, Portland cement, and blends of Portland cement with blast-furnace slag, metakaolin, or silica fume. Cem Concr Res 2004;34(9):1733–77.
[12] Puertas F, Fernández-Jiménez A. Mineralogical and microstructural characterisation of alkali-activated fly ash/slag pastes. Cem Concr Compos 2003;25(3):287–92.
[13] Puertas F, Martínez-Ramírez S, Alonso S, Vázquez E. Alkali-activated fly ash/slag cement. Strength behaviour and hydration products. Cem Concr Res 2000;30:1625–32.
[14] Yip CK, Lukey GC, Provis JL, van Deventer JSJ. Effect of calcium silicate sources on geopolymerisation. Cem Concr Res 2008;38(4):554–64.
[15] Yip CK, van Deventer JSJ. Microanalysis of calcium silicate hydrate gel formed within a geopolymeric binder. J Mater Sci 2003;38(18):3851–60.
[16] Yip CK, Lukey GC, van Deventer JSJ. The coexistence of geopolymeric gel and calcium silicate hydrate at the early stage of alkaline activation. Cem Concr Res 2005;35(9):1688–97.
[17] Duxson P, Provis JL. Designing precursors for geopolymer cements. J Am Ceram Soc 2008;91(12):3864–9.
[18] van Deventer JSJ, Provis JL, Duxson P, Brice DG. Chemical research and climate change as drivers in the commercial adoption of alkali activated materials. Waste Biomass Valoriz 2010;1(1):145–55.
[19] Bernal SA. Carbonatación de Concretos Producidos en Sistemas Binarios de una Escoria Siderúrgica y un Metacaolín Activados Alcalinamente. Ph.D. Thesis. Universidad del Valle, Cali, Colombia; 2009.
[20] Buchwald A, Hilbig H, Kaps C. Alkali-activated metakaolin-slag blends–performance and structure in dependence on their composition. J Mater Sci 2007;42(9):3024–32.
[21] Alonso S, Palomo A. Alkaline activation of metakaolin and calcium hydroxide mixtures: influence of temperature, activator concentration and solids ratio. Mater Lett 2001;47(1–2):55–62.
[22] Granizo ML, Alonso S, Blanco-Varela MT, Palomo A. Alkaline activation of metakaolin: effect of calcium hydroxide in the products of reaction. J Am Ceram Soc 2002;85(1):225–31.
[23] Bernal SA, Mejía de Gutierrez R, Rose V, Provis JL. Effect of silicate modulus and metakaolin incorporation on the carbonation of alkali silicate-activated slags. Cem Concr Res 2010;40(6):898–907.
[24] Kakali G, Perraki T, Tsivilis S, Badogiannis E. Thermal treatment of kaolin: the effect of mineralogy on the pozzolanic activity. Appl Clay Sci 2001;20(1–2): 73–80.
[25] Rahier H, Wullaert B, van Mele B. Influence of the degree of dehydroxylation of kaolinite on the properties of aluminosilicate glasses. J Therm Anal Calorim 2000;62(2):417–27.
[26] Torres J, Mejía de Gutiérrez R, Puertas F. Efecto de la temperatura de tratamiento de un caolín en la permeabilidad a cloruros en morteros. Mater Construcc 2007;57(285):61–9.
[27] White CE, Provis JL, Proffen T, Riley DP, van Deventer JSJ. Density functional modeling of the local structure of kaolinite subjected to thermal dehydroxylation. J Phys Chem A 2010;114(14):4988–96.
[28] Nocuń-Wczelik W. Heat evolution in alkali activated synthetic slag-metakaolin mixtures. J Thermal Anal Calorim 2006;86(3):739–43.
[29] Fernández-Jiménez A, Puertas F, Arteaga A. Determination of kinetic equations of alkaline activation of blast furnace slag by means of calorimetric data. J Thermal Anal Calorim 1998;52(3):945–55.
[30] Fernández-Jiménez A, Puertas F. Alkali-activated slag cements: kinetic studies. Cem Concr Res 1997;27(3):359–68.
[31] Shi C, Day RL. A calorimetric study of early hydration of alkali-slag cements. Cem Concr Res 1995;25(6):1333–46.
[32] Granizo ML, Blanco MT. Alkaline activation of metakaolin – an isothermal conduction calorimetry study. J Therm Anal 1998;52(3):957–65.
[33] Provis JL, van Deventer JSJ. Geopolymerisation kinetics. 2. Reaction kinetic modelling. Chem Eng Sci 2007;62(9):2318–29.
[34] Lloyd RR, Provis JL, van Deventer JSJ. Microscopy and microanalysis of inorganic polymer cements. 2: The gel binder. J Mater Sci 2009;44(2):620–31.
[35] Hewlett PC. Lea's chemistry of cement and concrete. 4th ed. Oxford, UK: Elsevier; 1998.
[36] Taylor HFW. Cement chemistry. 2nd ed. London, UK: Thomas; 1997.
[37] Rajaokarivony-Andriambololona Z, Thomassin JH, Baillif P, Touray JC. Experimental hydration of two synthetic glassy blast furnace slags in water and alkaline solutions (NaOH and KOH 0.1 N) at 40 °C: structure, composition and origin of the hydrated layer. J Mater Sci 1990;25(5):2399–410.
[38] Fernández-Jiménez A, Puertas F. Setting of alkali-activated slag cement. Influence of activator nature. Adv Cem Res 2001;13(3):115–21.
[39] Bakharev T, Sanjayan JG, Cheng Y-B. Alkali activation of Australian slag cements. 1999;29(1):113–20.
[40] Lootens D, Jousset P, Martinie L, Roussel N, Flatt RJ. Yield stress during setting of cement pastes from penetration tests. Cem Concr Res 2009;39(5):401–8.
[41] Krizan D, Zivanovic B. Effects of dosage and modulus of water glass on early hydration of alkali–slag cements. Cem Concr Res 2002;32(8):1181–8.
[42] Burciaga-Díaz O, Escalante-García JI, Arellano-Aguilar R, Gorokhovsky A. Statistical analysis of strength development as a function of various parameters on activated metakaolin/slag cements. J Am Ceram Soc 2010;93(2):541–7.
[43] Roy DM, Silsbee MR. Alkali activated materials. An overview. Mater Res Soc Symp Proc 1992;245:153–64.
[44] Wang SD, Scrivener KL. Hydration products of alkali-activated slag cement. Cem Concr Res 1995;25(3):561–71.
[45] Bonk F, Schneider J, Cincotto MA, Panepucci H. Characterization by multinuclear high-resolution NMR of hydration products in activated blast-furnace slag pastes. J Am Ceram Soc 2003;86(10):1712–9.
[46] Brough AR, Atkinson A. Sodium silicate-based, alkali-activated slag mortars. Part I. Strength, hydration and microstructure.. Cem Concr Res 2002;32:865–79.
[47] Escalante-Garcia J, Fuentes AF, Gorokhovsky A, Fraire-Luna PE, Mendoza-Suarez G. Hydration products and reactivity of blast-furnace slag activated by various alkalis. J Am Ceram Soc 2003;86(12):2148–53.
[48] Fernández-Jiménez A, Puertas F. Structure of calcium silicate hydrates formed in alkaline-activated slag: influence of the type of alkaline activator. J Am Ceram Soc 2003;86(8):1389–94.
[49] Zhou H, Wu X, Xu Z, Tang M. Kinetic study on hydration of alkali-activated slag. Cem Concr Res 1993;23:1253–8.
[50] Zhang YJ, Zhao YL, Li HH, Xu DL. Structure characterization of hydration products generated by alkaline activation of granulated blast furnace slag. J Mater Sci 2008;43:7141–7.
[51] Yip CK, Lukey GC, Provis JL, van Deventer JSJ. Carbonate mineral addition to metakaolin-based geopolymers. Cem Concr Compos 2008;30(10):979–85.
[52] Farmer VC. The infrared spectra of minerals. London: Mineralogical Society; 1974.
[53] Gadsden JA. Infrared spectra of minerals and related inorganic compounds. London: Butterworths; 1975.
[54] Huang CK, Kerr PF. Infrared study of the carbonate minerals. Am Miner 1960;45(2):311–24.
[55] Sitarz M, Handke M, Mozgawa W. Identification of silicooxygen rings in SiO_2 based on IR spectra. Spectrochim Acta A 2000;56:1819–23.
[56] Sitarz M, Handke M, Mozgawa W, Galuskin E, Galuskina I. The non-ring cations influence on silicooxygen ring vibrations. J Mol Struct 2000;555:357–62.
[57] Yu P, Kirkpatrick RJ, Poe B, McMillan PF, Cong X. Structure of calcium silicate hydrate (C–S–H): near-, mid-, and far-infrared spectroscopy. J Am Ceram Soc 1999;82(3):742–8.
[58] Provis JL, Duxson P, Lukey GC, van Deventer JSJ. Statistical thermodynamic model for Si/Al ordering in amorphous aluminosilicates. Chem Mater 2005;17(11):2976–86.